Journal of
Materials Chemistry A

PAPER

View Article Online
View Journal | View Issue

Cite this: *J. Mater. Chem. A*, 2015, **3**, 3627

Hydrothermally synthesized Cu_xO as a catalyst for CO oxidation

Mu Yao Guo,[ab] Fangzhou Liu,[b] Jenkin Tsui,[c] Albert A. Voskanyan,[c]
Alan Man Ching Ng,*[ab] Aleksandra B. Djurišić,*[b] Wai Kin Chan,[c] Kwong-Yu Chan,[c]
Changzhong Liao,[d] Kaimin Shih[d] and Charles Surya[e]

Received 11th December 2014
Accepted 23rd December 2014

DOI: 10.1039/c4ta06804a

www.rsc.org/MaterialsA

Hydrothermally synthesized Cu_xO exhibited improved performance for CO oxidation compared to the hydrothermally synthesized Cu_2O, as well as commercial CuO nanoparticles. Hydrothermally synthesized Cu_xO predominantly consists of CuO, but it also contains a small contribution from Cu_2O, as well as $Cu_2(OH)_3(NO_3)$ (before annealing). After annealing, only CuO and Cu_2O phases are present, and the T_{50} value is significantly improved from 179 °C to 149 °C, and the T_{50} value of annealed hydrothermal Cu_xO remains practically unchanged for 3 catalytic cycles. The improved performance of hydrothermal Cu_xO can be attributed to its composition and surface properties. The ratio of lattice oxygen to surface oxygen (oxygen in surface adsorbates, surface states, and defects) increases after the first CO oxidation reaction for all samples except commercial CuO nanoparticles, which exhibit steady decrease with increased cycling. In addition, pure Cu_2O irreversibly changes to CuO after CO oxidation reaction, but its catalytic performance after the first cycle is significantly improved compared to commercial CuO nanoparticles.

Introduction

Carbon monoxide oxidation is a catalytic reaction of significant practical and theoretical interest.[1–4] It is necessary for minimizing CO emissions from vehicle exhausts, and it is also a common model reaction for studying heterogeneous catalysis.[4] Therefore, CO oxidation over different catalyst materials or catalyst/support combinations has been extensively studied.[1–21] Among various materials which are of interest as CO oxidation catalysts, noble metals have been commonly investigated.[1,2] Noble metals typically exhibit high activity for low temperature CO oxidation,[1,4] but due to their high cost there is considerable interest in exploring the use of less expensive materials as catalysts for CO oxidation. A common approach in using a noble metal catalyst is to use a metal oxide support. However, in addition to possible use as supports, some metal oxides, such as copper oxides and cobalt oxide, also exhibit significant activity for CO oxidation.[1] Copper oxides are considerably more environmentally friendly materials compared to cobalt oxide. However, unsupported copper oxides have not been commonly used compared to cobalt oxide,[1] while there have been numerous studies on supported copper oxides as catalysts for CO oxidation.[1,7–9,11,17] This is partly due to the issues with stability and the variation in the oxidation state of copper.[1] However, the preparation of supported copper oxides is typically more complex, and thus a simple preparation of highly active and stable unsupported copper oxide catalysts is of significant interest.[14]

In copper oxides, copper can typically occur as Cu(I) in Cu_2O or Cu(II) in CuO. Cu_2O is commonly considered to be more active for CO oxidation,[1,21] although this has not been confirmed by all the studies.[1,13] This is likely due to the fact that surface states and defects can play a significant role in the activity of Cu_xO towards CO oxidation.[1] Furthermore, the morphology and heat treatment of CuO significantly affect its performance towards CO oxidation. It has been shown that T_{50} (temperature for 50% CO oxidation) of CuO can vary from 134 °C for mesoporous CuO pretreated at 200 °C to 190 °C for bulk CuO pretreated at 400 °C.[3] Consequently, different morphologies of copper oxide nanostructures have been studied such as CuO nanowires,[5,18] polyhedral Cu_2O microcrystals,[6] CuO nanocrystals with different shapes (nanoparticles, nanobelts, and nanoplatelets),[12] CuO porous microparticles,[13] CuO porous nanosheets,[14] Cu_2O concave microcrystals,[16] CuO nanoparticles,[15,19] and CuO nanorods.[20] The obtained performance towards CO oxidation considerably varied across the literature, depending on the composition, morphology and synthesis method of Cu_xO.

---

[a] Department of Physics, South University of Science and Technology of China, Shenzhen, China. E-mail: ngamc@sustc.edu.cn; Fax: +86-755-88018204; Tel: +86-755-88018211

[b] Department of Physics, The University of Hong Kong, Pokfulam Road, Hong Kong. E-mail: dalek@hku.hk; Fax: +852 2559 9152; Tel: +852 2859 7946

[c] Department of Chemistry, The University of Hong Kong, Pokfulam Road, Hong Kong

[d] Dept. of Civil Engineering, The University of Hong Kong, Pokfulam Road, Hong Kong

[e] Dept. of Electronic and Information Engineering, Hong Kong Polytechnic University, Hung Hom, Kowloon, Hong Kong

Thus, here, we studied the CO oxidation catalytic activity for different Cu_xO samples. We have focused on hydrothermal synthesis for unsupported Cu_xO catalysts as a simple, inexpensive, and easily scalable method of production. We compared the catalytic activity of hydrothermally synthesized Cu_xO (labeled as Cu_xO HT before annealing and Cu_xO HT A after annealing) and hydrothermally synthesized Cu_2O samples (labeled as Cu_2O), as well as commercial CuO nanoparticles (labeled as CuO NPs). We found that the hydrothermally synthesized Cu_2O exhibited the worst performance in the 1st cycle among all the samples, with lower catalytic activity compared to CuO, as well as inferior stability. However, after the conversion of Cu_2O to CuO in the 1st cycle, its performance is improved, and is comparable to the hydrothermally synthesized Cu_xO. However, the performance of commercial CuO NPs worsens after the 1st cycle and remains poor in the 2nd and 3rd cycles. The obtained results are discussed in detail.

Experimental section

Material synthesis

Copper nitrate trihydrate (purity ~98%) and hexamethylenetetramine (purity 99%) were obtained from Sigma-Aldrich. Ascorbic acid (99%) was obtained from Acros Organics. Sodium hydroxide (AR) was obtained from Dieckmann Chemistry. CuO nanoparticles (99%, APS 30–50 nm, sample CuO NPs) were obtained from Nanostructured & Amorphous Materials, Inc. CuO was prepared by hydrothermal growth according to a previously published procedure.[22] Briefly, 25 mM of copper nitrate trihydrate and hexamethylenetetramine solution were placed in a 45 ml Teflon-lined stainless steel autoclave at 90 °C for 3 hours. After cooling to room temperature, the black precipitates were washed with DI water and ethanol for 3 times, followed by drying in vacuum for 16 hours (sample Cu_xO HT). Then, the materials were annealed at 500 °C for 1 hour (sample Cu_xO HT A). Cu_2O nanocubes (sample Cu_2O) were prepared following a procedure reported by Zhang *et al.*[25] Briefly, 5 ml NaOH aqueous solution (2 mol l^{-1}) was added to 50 ml of $Cu(NO_3)$ aqueous solution (0.01 mol l^{-1}) at 55 °C. After stirring for 30 min, 5 ml of ascorbic acid solution (0.6 mol l^{-1}) was added. The mixed solution was then stirred for 5 hours. The reddish brown precipitates were washed with deionized water and ethanol 3 times, followed by drying in vacuum for 16 h.

Material characterization

The morphology and crystal structure of the samples were examined by scanning electron microscopy (SEM) using a JEOL JSM-7001F field emission SEM and X-ray diffraction (XRD) measurement using a Bruker AXS D8 ADVANCE diffractometer. A Micromeritics ASAP 2020 analyzer was used to carry out the Brunauer–Emmet–Teller (BET) surface area measurements using nitrogen as the adsorbent gas at 77 K. Copper oxide samples were degassed at 473 K overnight under the vacuum before the analysis. X-ray photoelectron spectroscopy (XPS) spectra were obtained using Physical Electronics 5600 multitechnique system. Fourier transform infrared spectroscopy (FTIR) measurements were performed in ambient atmosphere on KBr pellets containing Cu_xO samples using a PerkinElmer Spectrum Two IR Spectrometer. Infrared grade KBr (Sigma Aldrich Co.) was prebaked in a vacuum oven. A fixed amount of different Cu_xO samples was uniformly mixed with KBr and ground in a mortar followed by pressing into pellets using an evacuable pellet die (13 mm inner diameter) for FTIR measurement. The pellet was baked for 5 minutes before the measurement. Exposure time to ambient atmosphere was minimized for each sample.

Catalytic activity evaluation

For the measurement of catalytic activity, carbon monoxide oxidation reaction was carried out under atmospheric pressure in a Hiden CATALAB fixed-bed system using 30 mg of catalyst from 30 °C to 500 °C with a heating rate of 10 °C min^{-1}. The reaction mixture consisted of 4% CO and 4% O_2 with the balance helium as the carrier gas. The total flow rate of feed gas was 50 ml min^{-1}. Before starting the test, the system was purged with helium at 30 °C for 20 min, and then with feeding gas for another 20 min without any initial pretreatment of the catalyst. The outlet gas was analyzed by a mass spectrometer. The entire process was repeated for 3 times.

Results and discussion

Fig. 1 shows the SEM images of different Cu_xO samples, whereas TEM images with corresponding high resolution TEM images and selected area electron diffraction patterns are shown in Fig. 2. It can be observed that all CuO samples are polycrystalline with irregular shapes, while Cu_2O samples have a regular prism shape. Crystal structure was determined from XRD measurements, and the obtained results are shown in Fig. 3 and summarized in Table 1. Hydrothermally synthesized Cu_2O samples contain only Cu_2O phase. Commercial CuO NPs exhibit only CuO phase. The crystallite size obtained from XRD data is ~10 nm, which is considerably smaller than the nominal

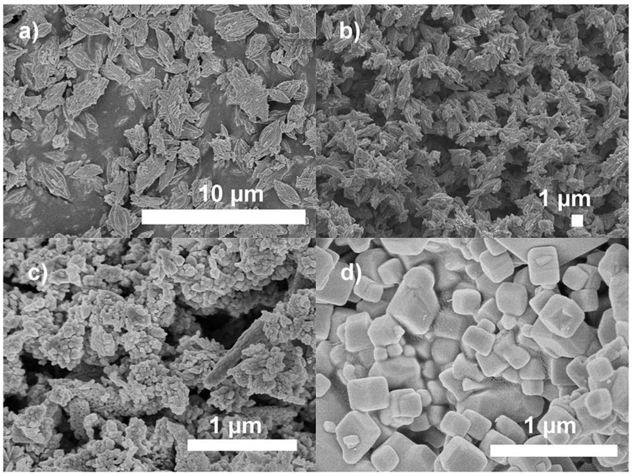

Fig. 1 SEM images of different cupric/cuprous oxide samples (a) Cu_xO HT, (b) Cu_xO HT annealed, (c) CuO NPs, and (d) Cu_2O.

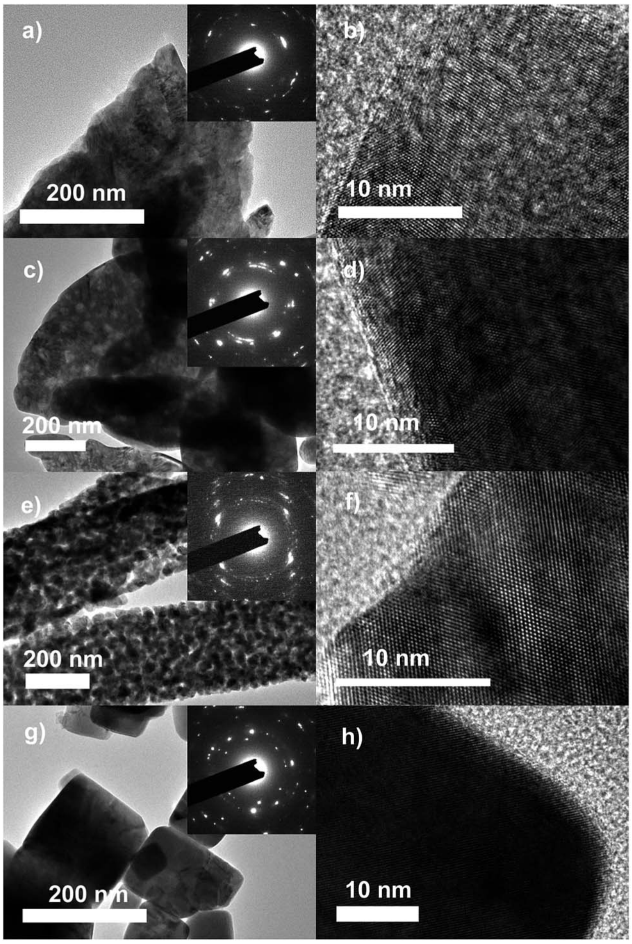

Fig. 2 TEM images of different cupric/cuprous oxide samples (a) Cu_xO HT, (b) high resolution TEM image of Cu_xO HT, (c) annealed Cu_xO HT, (d) high resolution TEM image of annealed Cu_xO HT, (e) CuO NPs, (f) high resolution TEM image of CuO NPs, (g) Cu_2O, (h) high resolution TEM image of Cu_2O. Insets show the corresponding SAED patterns.

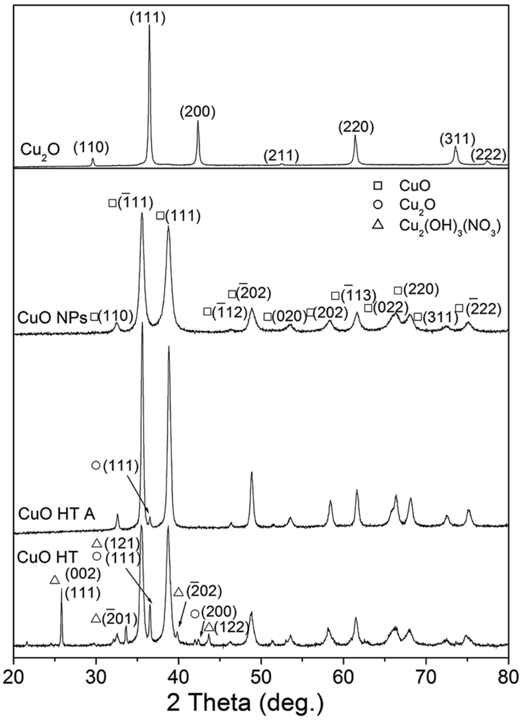

Fig. 3 XRD patterns of different cupric/cuprous oxide samples. Squares denote peaks corresponding to CuO (JCPDS file no. 80-0076), circles denote peaks corresponding to Cu_2O (JCPDS file no. 78-2076), while triangles denote peaks corresponding to $Cu_2(OH)_3(NO_3)$ (JCPDS file no. 75-1779).

Table 1 Crystallinity parameters of different CuO nanoparticles[a]

Sample	CuO (nm)	Cu_2O (nm)	$Cu_2(OH)_3(NO_3)$ (nm)
Cu_xO HT	14.7 ± 0.3	54	80 ± 5
Cu_xO HT A	23.9 ± 0.5	61	—
CuO NPs	10.2 ± 0.2	—	—
Cu_2O	—	34.5 ± 0.4	—

[a] The crystal size was calculated using double-Voigt approach, which was implemented in TOPAS 4.2 software.

Table 2 T_{50} and BET surface area of the different CuO nanoparticles

	T_{50} (1st) (°C)	T_{50} (2nd) (°C)	T_{50} (3rd) (°C)	BET surface area ($m^2\ g^{-1}$)
Cu_xO HT	179	140	140	3.55
Cu_xO HT A	149	150	150	1.90
CuO NPs	183	209	209	13.19
Cu_2O	192	131	142	3.09

particle size, in agreement with very large BET surface area, shown in Table 2. HT Cu_xO samples, however, exhibit mixed phases. The dominant phase is CuO, but the clear presence of Cu_2O as well as copper hydroxide nitrate can be detected. After annealing, the copper hydroxide nitrate phase is absent, and only CuO and Cu_2O phases are observed, with crystallite sizes of ~24 nm and ~61 nm, respectively. The crystallite size is the largest in the annealed HT Cu_xO samples, followed by HT Cu_xO samples before annealing, Cu_2O, and then CuO samples. The trends in BET surface area agree with expectations from crystallite sizes (smaller size = larger surface area).

CO oxidation experiments were conducted on different copper oxide samples, and the obtained results are shown in Fig. 4. We obtained improved CO oxidation performance for CuO compared to Cu_2O, in agreement with a previous study.[13] In addition, in a previous report on CO oxidation over Cu_2O microcrystals, all the samples exhibited T_{50} exceeding 200 °C,[16] in agreement with the observed higher conversion temperature for Cu_2O in our study (~192 °C). In comparison, the obtained T_{50} value for commercial CuO was ~183 °C. For hydrothermally grown Cu_xO, the T_{50} value improved dramatically after annealing from ~179 °C to ~149 °C. It can be observed that high BET surface area does not guarantee high catalytic activity because the BET surface area of CuO NPs is several times higher than that of any other samples, while this sample does not exhibit high catalytic activity. Furthermore, the activity of CuO NPs

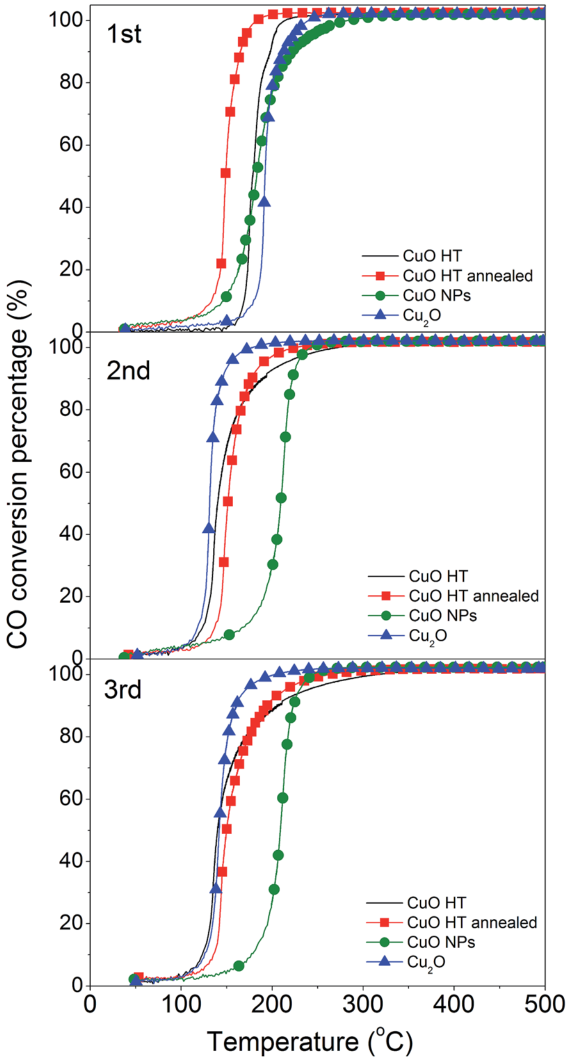

Fig. 4 CO oxidation conversion percentages over different cupric/cuprous oxide catalysts.

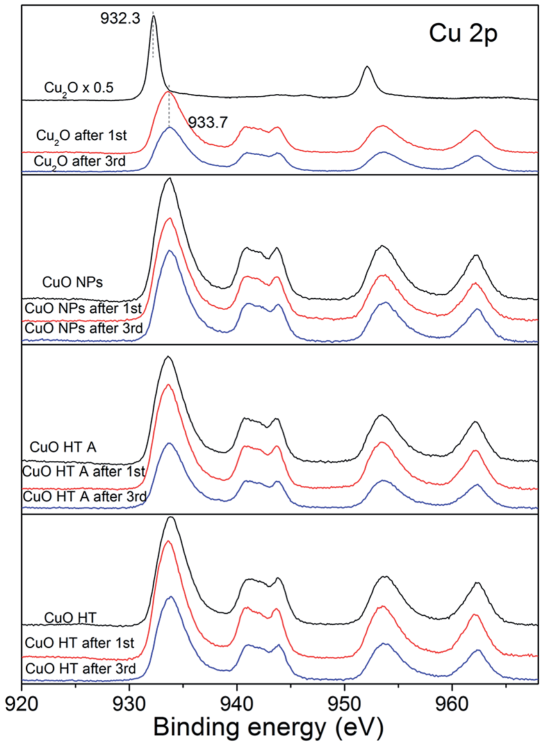

Fig. 5 Cu 2p XPS peaks of different cupric/cuprous oxide samples.

worsened after the 1st cycle, as summarized in Table 2. The Cu$_x$O HT-A sample exhibited stable performance for 3 cycles with no significant changes in the activity, while the activity of Cu$_x$O HT and Cu$_2$O improved significantly after the first cycle. However, T_{50} remained the same for the 2nd and 3rd cycles for Cu$_x$O HT A, while it increased after the second cycle for Cu$_2$O.

To further investigate the composition of different copper oxide samples and the reasons for the improvement in catalytic performance for the annealed HT samples, XPS and FTIR measurements were performed before and after CO oxidation. The obtained results for Cu 2p and O 1s peaks are shown in Fig. 5 and 6, respectively, and summarized in Table 3. The FTIR spectra are shown in Fig. 7. Cu 2p spectra for all the samples except pure Cu$_2$O exhibit features characteristic of bulk CuO.[20,24,26,27] For CuO NPs, as well as Cu$_x$O HT samples (before and after annealing), no significant shift of the main Cu peak compared to the bulk CuO value (~933.8 eV)[20] is observed. HT samples show a slightly lower peak position of ~933.6 eV, which is likely due to the small presence of Cu$_2$O (pure Cu$_2$O samples exhibit a peak at ~932.3 (ref. 23)). We can also observe that after CO oxidation, Cu$_2$O changes to CuO. For the other two samples, there are no significant changes in Cu 2p spectra before and after CO oxidation reaction. In some samples

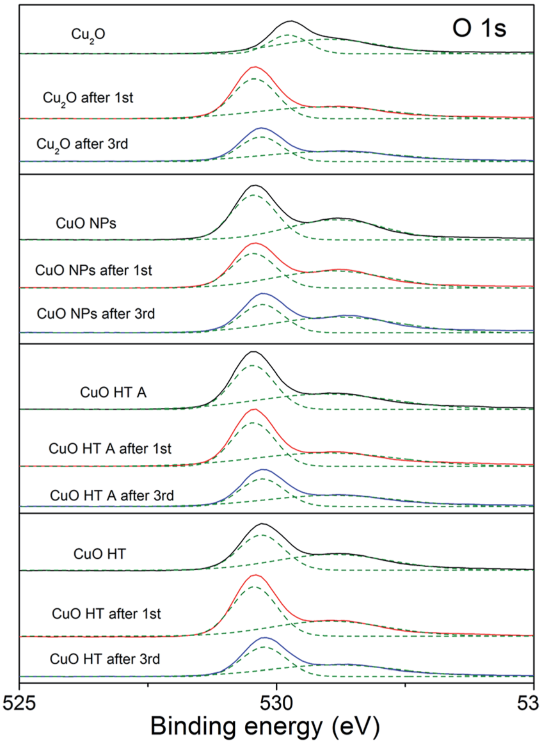

Fig. 6 O 1s XPS peak of different cupric/cuprous oxide samples.

Table 3 Composition of different Cu_xO samples obtained from fitting the XPS spectra[26] before and after CO oxidation reaction

	O/Cu, before	O/Cu, after 1 cycle	O/Cu, after 3 cycles	O_l/O_s, before	O_l/O_s, after 1 cycle	O_l/O_s, after 3 cycles
Cu_xO HT	1.20	1.27	1.19	0.92	1.38	0.88
Cu_xO HT A	1.27	1.16	1.36	1.11	1.21	1.00
CuO NPs	1.33	1.23	1.46	1.19	0.98	0.68
Cu_2O	0.63	1.14	1.18	0.55	1.45	0.78

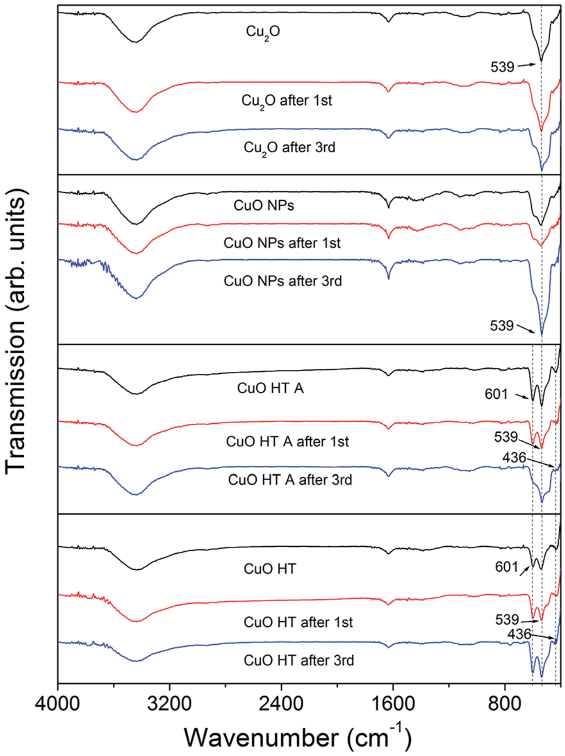

Fig. 7 FTIR spectra of different cupric/cuprous oxide samples.

(CuO HT, CuO NPs, and Cu_2O) small peak shifts (±0.1) can be observed for spectra obtained after the 1^{st} and after the 3^{rd} cycle, but it was not possible to obtain any Cu^+ contributions by fitting the peaks with two Gaussians.[19]

More significant differences, however, can be observed in O 1s peak. The O 1s peak typically consists of two peaks, with the lower energy peak (labeled as O_l) attributed to lattice oxygen O^{2-}, while the broad higher energy peak (labeled as O_s) could originate from hydroxyl groups, surface states, surface adsorbed oxygen, and/or oxygen defect sites.[15,19,20] Because the peak is broad, it likely arises from the multiple contributions of different types of adsorbed oxygen/oxygen defects.[20] The change observed for Cu_2O samples is consistent with the change of the sample structure from Cu_2O to CuO. All the samples with the dominant CuO phase exhibit a high O/Cu ratio, which is not significantly affected (±0.1) by the CO oxidation reaction in the first cycle, as shown in Table 3. The O_l/O_s ratio decreases for CuO NPs, while it increases for both Cu_xO HT samples. The change is more significant for the samples before annealing. After 3 cycles, there is a decrease in O_l/O_s ratio in all samples compared to the composition after the 1^{st} cycle. However, the O_l/O_s ratio is substantially lower compared to the sample before CO oxidation only for the CuO NP sample, where a steady decrease in O_l/O_s ratio is observed with increased cycling. The annealed HT Cu_xO samples show very small changes in O/Cu and O_l/O_s ratios after CO oxidation reaction. This confirms the stability of the annealed HT Cu_xO as a catalyst for CO oxidation because for a full catalytic cycle, it is necessary to have a recovery of two oxygen species.[26]

In the FTIR spectra, we can observe modes characteristic of CuO (at ~436 cm^{-1} and ~601 cm^{-1}, with the expected peak at ~497 cm^{-1} not clearly resolved).[28] The mode at ~539 cm^{-1} can also be assigned to CuO.[29] The modes corresponding to Cu_2O (627 cm^{-1} and ~619 cm^{-1})[29] could not be clearly resolved. Other clear vibration modes in the spectra correspond to OH group and water vibrations.[30] No clear trends could be observed in the relationship between FTIR spectra and CO oxidation activity.

From the obtained results, it is obvious that hydrothermally synthesized samples regardless of their initial composition exhibit high catalytic activity towards CO oxidation after the first cycle. The annealed HT Cu_xO also exhibits excellent stability. It is well known that the surface states (surface oxygen in particular) and the oxidation state of copper play a significant role in the catalytic activity towards CO oxidation.[26,27,31–33] All the samples after cycling exhibit large O/Cu ratios. Thus, it is possible that a significant amount of oxygen is adsorbed on the surface, which can contribute to the enhanced catalytic activity.[20] High catalytic activity of CuO nanorods was previously attributed to poor crystallization, resulting in the participation of adsorbed oxygen in the reaction instead of lattice oxygen.[20] However, a large O/Cu ratio also applies to CuO NPs, which exhibit inferior catalytic activity despite their significantly higher BET surface area compared to all the hydrothermally synthesized samples. The significant difference that we can observe between CuO NPs and hydrothermally synthesized samples is the steady decrease of O_1/O_s with increased cycling. This indicates that hydrothermally synthesized samples possibly contain more active sites related to oxygen surface states and that these sites can remain stable in the annealed samples (possibly due to the desorption of less stable species during annealing).

Conclusions

We have prepared unsupported Cu_xO catalysts using a simple hydrothermal synthesis method, which is inexpensive and easily scalable. The hydrothermally synthesized Cu_2O is converted to CuO after the first cycle of CO oxidation. After one cycle, three hydrothermally synthesized samples exhibit comparable performance, which is significantly better than that of pure CuO nanoparticles. In addition, the annealed HT Cu_xO samples exhibit very stable performance with repeated cycling. The improved catalytic performance can likely be attributed to the presence of a small amount of Cu_2O in hydrothermally synthesized samples and the presence of surface oxygen states.

Acknowledgements

Financial support from the Clean Energy Strategic Research Theme, Initiative on Clean Energy and Environment (ICEE), University Development Fund, Seed Funding Grant (of the University of Hong Kong) and RGC GRF grant HKU 701910 is acknowledged. Partial support of the work is provided by the RGC Theme-based Research Scheme (Grant number: HKU T23-713/11). AMCN would like to acknowledge the support from a grant from Shenzhen Science and Technology Commission (Project no. JCYJ20120830154526542) and National Science Fund of China (Project No. 21403103).

Notes and references

1 S. Royer and D. Duprez, *ChemCatChem*, 2011, **3**, 24.
2 S. A. C. Carabineiro, N. Bogdanchikova, M. Avalos-Borja, A. Pestryakov, P. B. Tavares and J. L. Figueiredo, *Nano Res.*, 2011, **4**, 180.
3 Y. Ren, Z. Ma, L. Qian, S. Dai, H. He and P. G. Bruce, *Catal. Lett.*, 2009, **131**, 146.
4 Z. Z. Wei, D. C. Li, X. Y. Pang, C. Q. Lv and G. C. Wang, *ChemCatChem*, 2012, **4**, 100.
5 Y. Feng and X. Zheng, *Nano Lett.*, 2010, **10**, 4762.
6 M. Leng, M. Liu, Y. Zhang, Z. Wang, C. Yu, X. Yang, H. Zhang and C. Wang, *J. Am. Chem. Soc.*, 2010, **132**, 17084.
7 F. Balıkçı Derekaya, C. Kutar and Ç. Güldür, *Mater. Chem. Phys.*, 2009, **115**, 496.
8 J. L. Cao, G. S. Shao, Y. Wang, Y. Liu and Z. Y. Yuan, *Catal. Commun.*, 2008, **9**, 2555.
9 M. F. Luo, Y. P. Song, J. Q. Lu, X. Y. Wang and Z. Y. Pu, *J. Phys. Chem. C*, 2007, **111**, 12686.
10 C. Song, C. Wang, H. Zhu, X. Wu, L. Dong and Y. Chen, *Catal. Lett.*, 2008, **120**, 215.
11 B. White, M. Yin, A. Hall, D. Le, S. Stolbov, T. Rahman, N. Turro and S. O'Brien, *Nano Lett.*, 2006, **6**, 2095.
12 K. Zhou, R. Wang, B. Xu and Y. Li, *Nanotechnology*, 2006, **17**, 3939.
13 U. R. Pillai and S. Deevi, *Appl. Catal., B*, 2006, **64**, 146.
14 H. Huang, L. Zhang, K. Wu, Q. Yu, R. Chen, H. Yang, X. Peng and Z. Ye, *Nanoscale*, 2012, **4**, 7832.
15 J. H. Park, J. H. Cho, K. H. Cho, T. W. Lee, H. S. Han and C. H. Shin, *Korean J. Chem. Eng.*, 2012, **29**, 1151.
16 X. Wang, C. Liu, B. Zheng, Y. Jiang, L. Zhang, Z. Xie and L. Zheng, *J. Mater. Chem. A*, 2013, **1**, 282.
17 M. Y. Kang, H. J. Yun, S. Yu, W. Kim, N. D. Kim and J. Yi, *J. Mol. Catal. A: Chem.*, 2013, **368**, 72.
18 H. Yan, X. Liu, R. Xu and P. Zhao, *Mater. Res. Bull.*, 2013, **48**, 2102.
19 D. A. Svintsitskiy, A. P. Chupakhin, E. M. Slavinskaya, O. A. Stonkus, A. I. Stadnichenko, S. V. Koscheev and A. I. Boronin, *J. Mol. Catal. A: Chem.*, 2013, **368**, 95.
20 K. Zhong, J. Xue, Y. Mao, C. Wang, T. Zhai, P. Liu, X. Xia, H. Li and Y. Tong, *RSC Adv.*, 2012, **2**, 11520.
21 T. J. Huang and D. H. Tsai, *Catal. Lett.*, 2003, **87**, 173.
22 D. Li, Y. H. Leung, A. B. Djurišić, Z. T. Liu, M. H. Xie, J. Gao and W. K. Chan, *J. Cryst. Growth*, 2005, **282**, 105.
23 C. K. Wu, M. Yin, S. O'Brien and J. T. Koberstein, *Chem. Mater.*, 2006, **18**, 6054.
24 A. I. Stadnichenko, A. M. Sorokin and A. I. Boronin, *J. Struct. Chem.*, 2008, **49**, 341.
25 D. F. Zhang, H. Zhang, L. Guo, K. Zheng, X. D. Han and Z. Zhang, *J. Mater. Chem.*, 2009, **19**, 5220.
26 D. A. Svintsitskiy, A. I. Stadnichenko, D. V. Demidov, S. V. Koscheev and A. I. Boronin, *Appl. Surf. Sci.*, 2011, **257**, 8542.
27 D. A. Svintsitskiy, T. Y. Kardash, O. A. Stonkus, E. M. Slavinskaya, A. I. Stadnichenko, S. V. Koscheev, A. P. Chupakin and A. I. Boronin, *J. Phys. Chem. C*, 2013, **117**, 14588.
28 A. S. Ethiraj and D. J. Kang, *Nanoscale Res. Lett.*, 2012, **7**, 70.
29 M. R. Johan, M. S. M. Suan, N. L. Hawari and H. Y. Ching, *Int. J. Electrochem.*, 2011, **6**, 6094.
30 D. P. Dubal, D. S. Dhawale, R. R. Salunkhe, V. S. Jamdade and C. D. Lokhande, *J. Alloys Compd.*, 2010, **492**, 26.
31 V. A. Sadykov, S. F. Tikhov, N. N. Bulgakov and A. P. Gerasev, *Catal. Today*, 2009, **144**, 324.
32 T.-J. Huang and D.-H. Tsai, *Catal. Lett.*, 2003, **87**, 173.
33 K. Nagase, Y. Zheng, Y. Kodama and J. Kakuta, *J. Catal.*, 1999, **187**, 123.